

JumpRoACH: A Trajectory-Adjustable Integrated Jumping–Crawling Robot

Gwang-Pil Jung , Carlos S. Casarez, Jongeun Lee, Sang-Min Baek, So-Jung Yim, Soo-Hwan Chae, Ronald S. Fearing, and Kyu-Jin Cho 

Abstract—In this paper, we present a milliscale-integrated jumping–crawling robot that can adjust its launch trajectory and upright itself. This multimodal robot shows an enhanced performance of overcoming obstacles compared with a robot with a single locomotion mode. To make this possible, the robot uses a newly developed jumping module with improved energy storing capacity and a height-adjustable active clutch. The jumping module utilizes both linear springs and torsional springs to maximize the energy-storing capacity under the given limit of structural robustness. To adjust the quantity of stored energy and release the energy at any state, an active clutch mechanism based on a single dc motor is developed, which enables the robot to control both jump timing and height. Also, an active shell allows the robot to upright itself after landing and to continue jumping and crawling. The jumping module and the shell are integrated with the lightweight VelociRoACH crawler. To show the usability in real-world applications, the integrated jumping–crawling robot is tested on the cluttered terrain. In result, the robot reaches a target using jumping, crawling, and self-righting.

Index Terms—Bioinspired robot, crawling robot, jumping robot, multimodal robot, self-right.

I. INTRODUCTION

RECENT studies on milliscale mobile robots have focused on increasing their maneuverability by modifying from

Manuscript received June 11, 2018; revised February 13, 2019; accepted March 17, 2019. Date of publication March 27, 2019; date of current version June 14, 2019. Recommended by Technical Editor Y. Hurmuzlu. This work was supported in part by the National Research Foundation (NRF-2016R1A5A1938472 and NRF-2017R1C1B5017816), and in part by a grant to Bio-Mimetic Robot Research Center funded by Defense Acquisition Program Administration (Grant UD130070ID). (*Corresponding author: Kyu-Jin Cho.*)

G.-P. Jung is with the Department of Mechanical and Automotive Engineering, SeoulTech, Seoul 01811, South Korea (e-mail: gpjung@seoultech.ac.kr).

C. S. Casarez is with the Systems Analyst Group, Intuitive Surgical, Sunnyvale, CA 94086 USA (e-mail: casarezc@berkeley.edu).

J. Lee, S.-M. Baek, S.-J. Yim, S.-H. Chae, and K.-J. Cho are with the Biorobotics Laboratory, Department of Mechanical Engineering, Seoul National University, Seoul 08826, South Korea (e-mail: yhjelee@snu.ac.kr; bsm6656@snu.ac.kr; yimsj94@gmail.com; justices@snu.ac.kr; kjcho@snu.ac.kr).

R. S. Fearing is with the Department of Electrical Engineering and Computer Sciences, University of California, Berkeley, Berkeley, CA 94720 USA (e-mail: ronf@eecs.berkeley.edu).

This paper has supplementary downloadable material available at <http://ieeexplore.ieee.org>, provided by the authors.

Color versions of one or more of the figures in this paper are available online at <http://ieeexplore.ieee.org>.

Digital Object Identifier 10.1109/TMECH.2019.2907743

TABLE I
JUMPING–CRAWLING ROBOTS

Robots	Mass (g)	Size (cm)	Jumping height (m)	Jumping distance (m)
Scout [7]	200	11.5	0.57	-
MiniWhegs [11]	191.4	10.4	0.18	-
JumpRoACH	99.0	12.0	1.5	0.8

single locomotion modes, such as crawling, climbing, and jumping, to multimodal locomotion that integrates multiple motions. Milliscale mobile robots with multiple motions have usually been developed for two purposes: saving the cost of transport (CoT) and expanding locomotion domain.

Integrated jumping and gliding is the representative multimodal locomotion for jump-gliding robots to reduce CoT [2]–[6]. Jump-gliding robots can extend the travelling distance in the horizontal direction for a given amount of stored energy. In case of expanding locomotion domain, robots often use an integrated jumping and crawling [7]–[12]. Such integrated locomotion can be easily seen in tiny insects, such as froghoppers, grasshoppers, and locusts. In ordinary situations, they use four forelegs to walk and crawl. When predators approach them, or they try to reach places they cannot crawl, they utilize their relatively long and thick hind legs.

To improve maneuverability like the insects mentioned above, some researchers have proposed milliscale robots that integrate jumping and crawling locomotion. Scout robot has two wheels for rolling and a winch for jumping [7]. The robot uses spring steel foot and jumps up to 30 cm. While the Scout robot has separate motions of jumping and rolling, the Mini-Whegs shows the integrated running and jumping locomotion. The Mini-Whegs overcomes a step by jumping up to 18 cm while also crawling [11]. Those robots have successfully shown the potential to expand locomotion domain by integrating two locomotions. Owing to the limited performance of jumping, as shown in Table I, however, there is still room for utilizing benefits of the integrated jumping–crawling locomotion.

To investigate the solution to increase energy-storing capacity, we examine the properties of milliscale jumping robots developed up to date and their jumping performance, as shown in Table II. Most jumping robots employ metal-based linear springs or torsional springs that are easy to obtain off the shelf. Unlike them, deformable robot [13] and closed elastica jumping robot [14] used metal strap as the energy-storing material.

TABLE II
PROPERTIES OF JUMPING ROBOTS

<i>Jumping robots</i>	<i>Size (cm)</i>	<i>Mass (g)</i>	<i>Jumping height (m)</i>	<i>Jumping distance (m)</i>	<i>Take-off velocity (m/s)</i>	<i>Height-Adjustability</i>	<i>Energy-storing component</i>	<i>Energy density¹ (J/kg)</i>
Flea [15]	2	1.1	0.64	0.7	4.2	Maybe, yes	SMA spring	9
Grillo (2007) [23]	3	10	-	-	3.6	No	linear spring	6
Grillo (2012) [24]	5	22	0.1	20	1.7	No	linear spring	1
7g jumping robot [19]	5	6.98	1.38	0.79	5.9	No	torsional spring	17.4
MSU Jumper 1 [8]	6.5	23.5	0.55	-	4.3	No	torsional spring	9
MSU Jumper 2 [18]	9	25	1.436	0.593	-	No	carbon strap	16
Deformable robot [13]	9	5	0.18	-	-	Yes	metal strap	1.8
Closed elastica [14]	11	18	0.15	0.95	-	No	metal strap	5
Proposed mechanism	11.5	42.6	2.75	0	7.86	Yes	torsional spring & latex rubber	30.9
Minimalist Jumping Robot [1]	15	1300	0.9	2	-	No	linear spring	12
TAUB [25], [26]	19	22.6	3.1	3	9	No	torsional spring	41.2
MultimoBat [2], [6]	28	115.6	3.65	-	-	Yes	linear spring	34.89

¹ Energy density is calculated based on take-off velocity, jumping height, and distance.

Flea-inspired jumping robot [15] employed shape memory alloy (SMA) spring actuators, which is known as high power-mass density material [16], [17]. The MSU jumper [18] has changed the energy-storing material from the steel torsional spring to the carbon fiber strap since the carbon fiber strap is lightweight and has large Young's modulus. After changing the material, they could increase the energy density of the robot from 9 to 14 J/kg. In terms of energy density, 7-g jumping robot [19] achieved 17.4 J/kg and could jump up to 1.38 m with 6.98-g mass. In case of small-scale hopping robots, they mostly employed series elastic actuation [20]–[22] and showed continuous jumping ability rather than focusing on jumping height.

To adjust the amount of energy storage is as important as to increase the energy-storing capacity, which enables the robot to control take-off speed and the jumping height. Previously, a variety of releasing mechanisms are employed, such as escapement-cam [19], one-way bearing [8], toothless gear [23], [24], latching [25], [26], buckling [14], and sparkler [27]. Those mechanisms have provided simple and effective solutions of energy storing and releasing but they always store the same amount of energy storage, which results in equal jumping height. To solve this issue, some of the jumping robots employed the concept of active clutch, which is useful for adjusting the amount of stored energy. Flea-inspired jumping robot employed two SMA coil actuators [15]. One is for storing the energy and the other is for triggering the jump. The deformable robot also used eight SMA coil actuators to store the elastic energy into the circular metal strap [13]. MultimoBat used one dc motor to store the energy by winding the wire [2]. To release the stored energy, an additional SMA wire actuator has been employed as an active clutch.

In this paper, we present an integrated jumping–crawling robot called JumpRoACH in Fig. 1 that can adjust its moving trajectory with improved jumping performance. Previously, we have proposed an integrated jumping–crawling robot [28]. The main difference between the previous version and the current

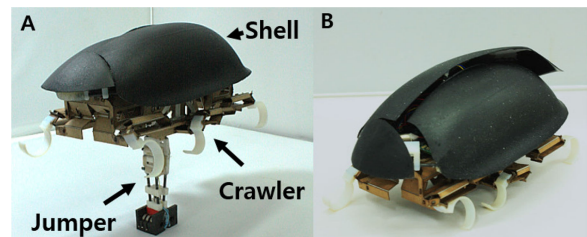


Fig. 1. JumpRoACH. (a) Jumping mode. (b) Crawling mode.

version is the energy-storing strategy. In the previous version, large displacement of latex rubber has been utilized to maximally store the energy. One serious problem, however, was the high peak loading force. The high peak loading force deteriorates structural robustness and shortens the lifespan of the jumping module when loading and unloading are repeated.

To solve this issue, a novel method of maximizing energy-storing capacity under given limit of structural robustness has been proposed. This main idea is applied to the newly developed jumping module and this jumping module is integrated with the lightweight crawling robot, VelociRoACH [29]. As a result, the robot can adjust moving trajectory by varying jumping height from 1.0 to 1.5 m and crawling speed from 0 to 0.56 m/s.

This paper consists of following contents: In design section, the idea of maximizing the jumper's energy-storing capacity is mainly described. The modeling section studies both statics and dynamics of the jumper to analyze the fast motion. In the experiment section, the performance of the jumping module and the integrated JumpRoACH is examined.

II. DESIGN

The jumping module is designed to fulfill two main requirements: First, the jumping module is required to have

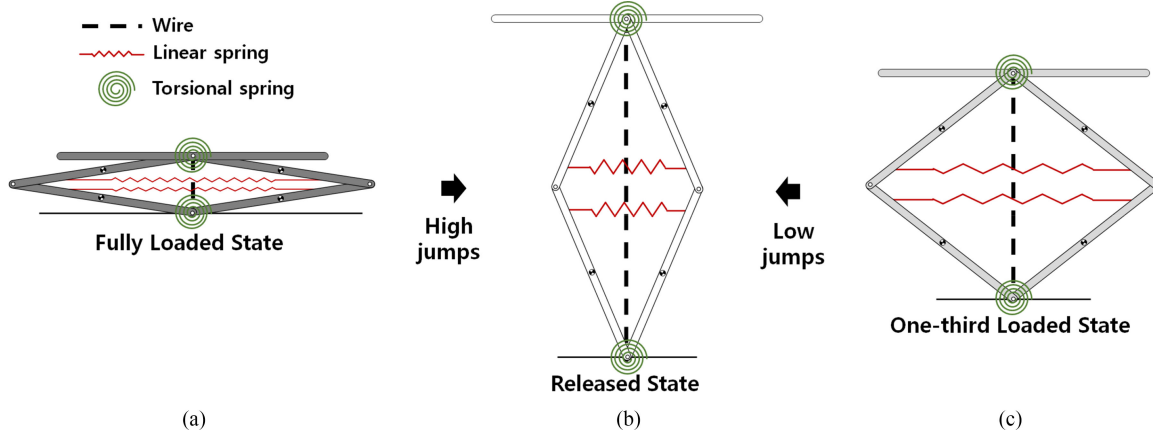


Fig. 2. Conceptual models of the proposed jumping mechanism in (a) the fully loaded state, (b) the released state, and (c) the one-third loaded state. The mechanism can jump from both the fully loaded state and the one-third loaded state depending on the required jumping heights.

energy-storing capacity as much as 50.0 J/kg (27 J in 40.0-g module) to enable the whole system to jump up to height of 1.5 m, assuming that the whole mass of the system is about 100.0 g. In milliscale jumping robots, the value of 50.0 J/kg is quite a large amount since the 7-g jumping robot [19], to our knowledge, has the largest energy-storing capacity of about 17.4 J/kg. We previously proposed an integrated jumping–crawling robot that weighs 59.4 g, jumps from 1.10 to 1.62 m, and crawls at a speed of 0 to 0.62 m/s [28]. To store the energy as much as possible, large displacement of latex rubber rather than large spring constant is utilized. This method, however, leads to the high peak loading force and tends to cause damage of the jumping module when loading and unloading are repeated. To solve this issue, a novel energy-storing strategy under limited structural robustness will be addressed.

The second design requirement is to make an active clutch that enables the jumping module to release the stored energy in any state, regardless of the amount of energy stored. By doing so, the jumping module can adjust the jumping speed. To make this possible, an active clutch mechanism using a single dc motor will be explained.

A. Structure of the Jumping Module

The jumping module has a fully foldable diamond-shaped four-bar linkage to install the structure inside the crawler's body. The structure has two types of energy storages, such as torsional springs and linear springs. The torsional springs are located at the top and the bottom of the four-bar linkage. At the center of the linkage, the linear springs are installed. As the structure is compressed, both the linear springs and the torsional springs deform, resulting in an increase of the amount of stored energy. Fig. 2(a) and (c) shows the jumping module with the full load of stored energy and one-third of its full capacity, respectively. In Fig. 2(b), the stored energy is released when the structure is decompressed.

Fig. 3 displays the entire jumping module. A wire is passing through the center of the structure, and a pulley winds the wire to fold the four-bar structure. At this time, the linear springs

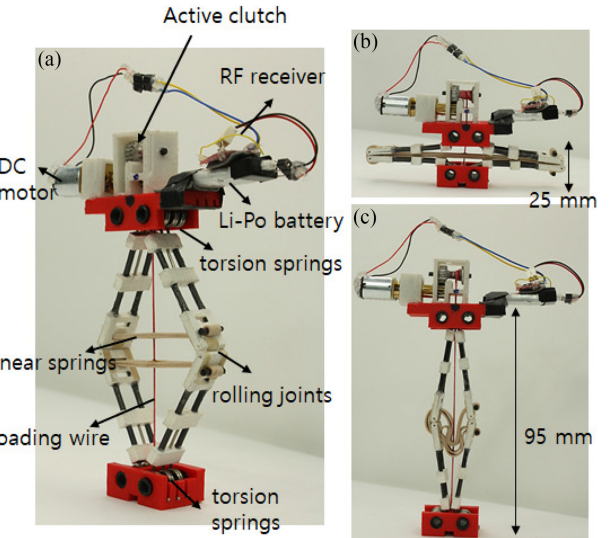


Fig. 3. (Left) Jumping module. (Top right) Fully loaded stated state. (Bottom right) Released state.

and the torsional springs store the elastic energy, as shown in Fig. 3(b).

B. Combined Types of Energy Storages

In short, to employ strong springs provide large energy-storing capacity. The jumping module, however, has a limit of structural robustness. In other words, the module has a high probability to fail when the strong springs are simply used. To maximize the storable energy under the given limit of structural robustness, the jumping module employs two different types of energy storages in terms of force-displacement relationship, as shown in Fig. 4. Fig. 4 shows the force-displacement curve of the linear spring, torsional spring, and the optimally combined case. In Fig. 4, the area under a curve stands for the amount of storable energy. Therefore, to maximize the area is important to boost the energy-storing capacity.

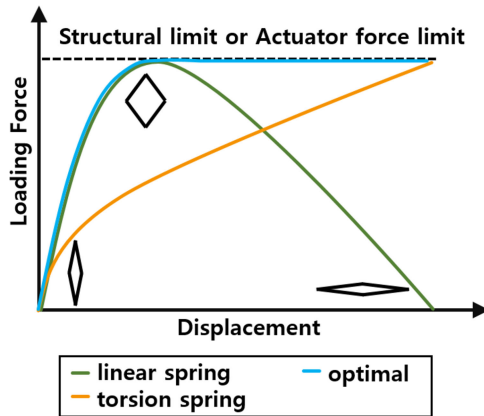


Fig. 4. Loading force versus displacement depending on types of energy storing methods.

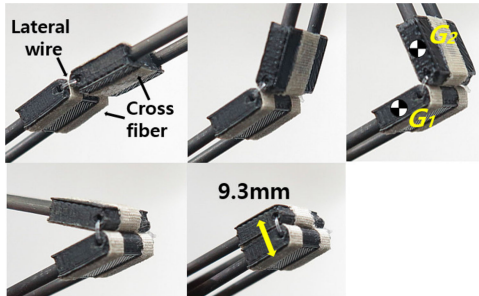


Fig. 5. Assembled rolling contact joint. The joint can be fully compressed just like human's knee.

In case of the linear spring, the loading force rapidly increases to the peak and decreases to zero according to the change in length of the moment arm. On the other hand, loading force of the torsion spring shows a modest increase, since loading force is simply proportional to the deformation of the spring. Based on these facts, the area under the limit can be maximally used when the two springs are appropriately combined, as shown in Fig. 4 (optimal case).

C. Rolling Contact Joints

The jumping module is required to be installed inside the crawler. Therefore, it is necessary to compress the module to the maximum so as not to interfere with the movement of the crawl. The extent to which the structure can be compressed is basically dependent on the range of motion of the joint. It is difficult for the structure to be completely compressed or decompressed when the joint has little range of motion. For this reason, as shown in Fig. 5, rolling and sliding joints have been developed like a human knee and applied to the side joints. In Fig. 5, the joint can be fully folded and unfolded. The joints are assembled using a lateral wire and three crossed straps. Basically, the lateral wire incorporates two linkages. The crossed strap prevents the joints from deviating from the center, as shown in Fig. 5 [30].

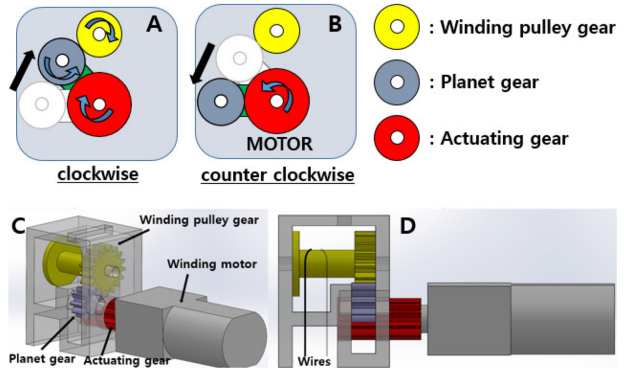


Fig. 6. (a) and (b) Conceptual diagram of the active triggering mechanism using a single dc motor. (c) and (d) 3-D description of the clutch mechanism.

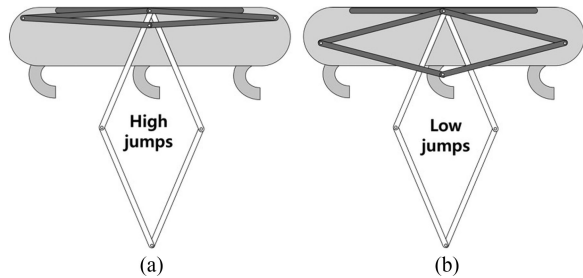


Fig. 7. Conceptual model of the height-adjustable integrated crawling-jumping robot, showing the state of the mechanism for (a) high jumps and (b) low jumps.

D. Height-Adjustable Triggering Mechanism

To release the energy is as important as to store the energy. To this end, an active clutch mechanism is proposed to enable the jumping module to release the stored energy in any state and accordingly to adjust the launching speed. The mechanism in Fig. 6 has three gears, such as a motor gear, a winding pulley gear, and a planet gear. The key working principle is energy storing and releasing depending on the rotating direction of the motor gear. When the motor gear rotates clockwise, the planet gear contacts the winding pulley gear and it begins to wind the wires, storing the energy. In case of counter-clockwise direction, the planet gear moves away from the winding pulley gear and the wound wire begins to loosen, resulting in the release of the stored energy. Thanks to this active clutch mechanism, the jumping module can release the energy at any state, as shown in Fig. 2, which enables the module to control its jumping speed.

E. Integration of Jumping and Crawling Mechanism

In Fig. 7, the jumping module is incorporated with a lightweight VelociRoACH crawler [29]. The crawler has an empty space inside the body of 110 mm length \times 20 mm width \times 30 mm depth. At this empty space, the jumping module is installed. When installing the jumping module, it is required to be positioned at the center to equally distribute the mass and to

TABLE III
MASS BUDGET

Components	Mass (g)
Carbon rods (8 ea)	2.0
Jumper transmission	4.8
Wire, joint rubber	2.2
Joints (8 ea)	4.0
Latex rubber for energy storage (2 ea)	2.2
Jumper motor	12.0
Li-Po battery	12.2
Control board	9.1
Crawler transmission	10.3
Crawler body	26.3
Shell including a motor	13.9
Total	99.0

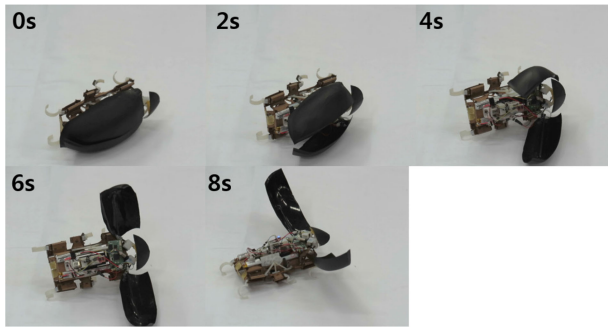


Fig. 8. Self-righting procedure using an active shell.

minimize the needless rotating motion. In Table III, the mass budget of the JumpRoACH is given.

The JumpRoACH adjusts the amount of the stored energy depending on the target jumping speed. In case of high jump shown in Fig. 7(a), the motor winds the wire until the jumper is fully compressed and maximally store the energy. In case of a low jump shown in Fig. 7(b), the motor slightly winds the wire and the jumping module is less compressed.

The dsPIC33JF128MC706-based board is used to control the JumpRoACH [31]. The board uses a wireless radio of 802.15.4 and two H-bridge motor drivers to control the crawling motors (MK07-3.3, Didel). For the jumper, a dc motor having the high gear ratio of 1000:1 (Pololu) is used to exert the high torque to the winding pulley gear.

F. Self-Righting Shell

When the robot moves around, the robot often turns over after jumping. To make the robot upright, an active shell structure (shown first by [32]) is installed at the upper side of the crawler. Fig. 8 shows how the shell operates. The shell consists of two wings. The wings are connected through bevel gears to operate them simultaneously. A small dc motor is installed at one side and to open and close the wings. By using the shell structure, the robot can stand upright no matter how it falls and continues jumping-crawling locomotion.

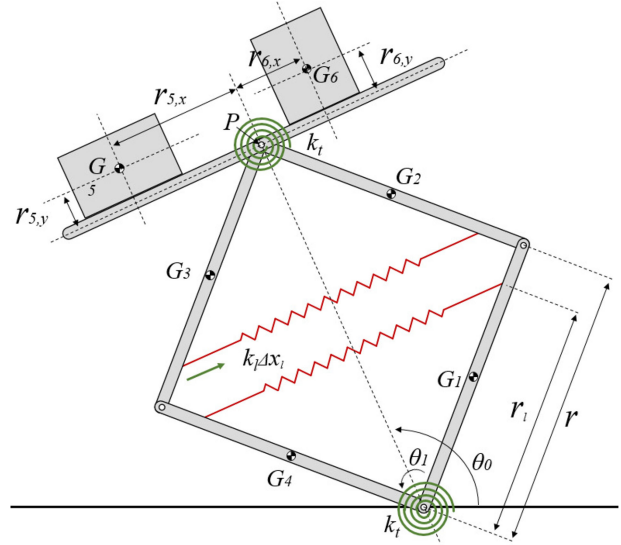


Fig. 9. Dynamic model of the proposed mechanism. G5 and G6 indicate the payload, such as a battery, electronics, and an actuator.

III. MODELING

In the previous section, to maximally use the area under the structural force limit is important for storing the energy as much as possible while ensuring structural safety. Therefore, to find out, the best combination of linear springs and torsional springs is required. To this end, we investigate the loading force through a static model. The loading force required to compress the jumping module is calculated based on the static model.

Dynamic analysis is also done based on the Lagrangian formulation since the take-off process of the module finishes within about 30 ms. Therefore, dynamic modeling is essentially required to investigate how the jumping module operates. Using the dynamic model, the take-off velocity, time, and released energy for jumping are given.

A. Loading Force Analysis

To choose the best combination of the linear springs and the torsional springs, the loading force is analyzed based on the static model, as shown in Fig. 9. In Fig. 9, the latex rubbers are positioned symmetrically at the upper triangle and the lower triangle. The torsional springs are located at the top and the bottom of the model. The loading force F is obtained using the moment equilibrium equation as follows:

$$rF\sin\theta' = r_1k_1\Delta x_1\cos\theta' + k_t\Delta\theta_1 \quad (1)$$

where θ_1 is the angle between the link 1 and 4, $\Delta x_i = r_i(\sin\theta' - \sin\theta'_{\text{initial}})$, $\theta' = \theta_1/2$, $\theta'_{\text{initial}} = \theta_{1,\text{initial}}/2$, and θ'_{initial} and $\theta_{1,\text{initial}}$ are the initial angles of θ' and θ_1 .

$$F = \frac{8r_1^2k_1(\sin\theta' - \sin\theta'_{\text{initial}})\cos\theta' + k_t\Delta\theta_1}{rs\sin\theta'} \quad (2)$$

where k_1 is a constant of the linear spring, k_t is a constant of the torsional spring, $r_1 = 41$ mm, $r = 45$ mm, and $\theta'_{\text{initial}} = 20^\circ$.

B. Dynamics

The jumping module is modeled with five links and four joints, as shown in Fig. 9. The model uses two generalized coordinates (θ_1 and θ_0) and accordingly is a two-degree-of-freedom system. Followings are the position of the links:

$$\vec{G}_1 = \begin{bmatrix} \frac{1}{2}r \cos(\theta_0 - \frac{1}{2}\theta_1) \\ \frac{1}{2}r \sin(\theta_0 - \frac{1}{2}\theta_1) \end{bmatrix} \quad (3)$$

where G_i is the position vector of each link, r is the length of each link

$$\vec{G}_2 = \begin{bmatrix} r \cos(\theta_0 - \frac{1}{2}\theta_1) + \frac{1}{2}r \cos(\theta_0 + \frac{1}{2}\theta_1) \\ r \sin(\theta_0 - \frac{1}{2}\theta_1) + \frac{1}{2}r \sin(\theta_0 + \frac{1}{2}\theta_1) \end{bmatrix} \quad (4)$$

$$\vec{G}_3 = \begin{bmatrix} r \cos(\theta_0 + \frac{1}{2}\theta_1) + \frac{1}{2}r \cos(\theta_0 - \frac{1}{2}\theta_1) \\ r \sin(\theta_0 + \frac{1}{2}\theta_1) + \frac{1}{2}r \sin(\theta_0 - \frac{1}{2}\theta_1) \end{bmatrix} \quad (5)$$

$$\vec{G}_4 = \begin{bmatrix} \frac{1}{2}r \cos(\theta_0 + \frac{1}{2}\theta_1) \\ \frac{1}{2}r \sin(\theta_0 + \frac{1}{2}\theta_1) \end{bmatrix} \quad (6)$$

$$\vec{G}_5 = \begin{bmatrix} r \cos(\theta_0 - \frac{1}{2}\theta_1) + r \cos(\theta_0 + \frac{1}{2}\theta_1) \\ -r_{5,y} \cos\theta_0 - r_{5,x} \sin\theta_0 \\ r \sin(\theta_0 - \frac{1}{2}\theta_1) + r \sin(\theta_0 + \frac{1}{2}\theta_1) \\ +r_{5,y} \sin\theta_0 + r_{5,x} \cos\theta_0 \end{bmatrix} \quad (7)$$

$$\vec{G}_6 = \begin{bmatrix} r \cos(\theta_0 - \frac{1}{2}\theta_1) + r \cos(\theta_0 + \frac{1}{2}\theta_1) \\ -r_{6,y} \cos\theta_0 + r_{6,x} \sin\theta_0 \\ r \sin(\theta_0 - \frac{1}{2}\theta_1) + r \sin(\theta_0 + \frac{1}{2}\theta_1) \\ +r_{6,y} \sin\theta_0 - r_{6,x} \cos\theta_0 \end{bmatrix} \quad (8)$$

where $r_{5,x}$, $r_{5,y}$, $r_{6,x}$, and $r_{6,y}$ are distances to the added masses

Based on the positions and the kinematic constraints, take-off of the jumping module is numerically analyzed by a Lagrange formulation. Following is the initial condition:

$$\theta_1 = 170^\circ \text{ in fully stored state.} \quad (9)$$

The jumping module takes off when the vertical reaction force, $V(t)$ in (11), is zero

$$m_{\text{robot}} a_{\text{robot},x} = \sum_{i=1}^6 m_i a_{i,x}(t) = -H(t) \quad (10)$$

$$m_{\text{robot}} a_{\text{robot},y} = \sum_{i=1}^6 m_i a_{i,y}(t) = V(t) - \sum_{i=1}^6 m_i g \quad (11)$$

where m_i is the mass of each link, a_{robot} is the acceleration of the mass center, a_i is the acceleration of each link, m_{robot} is the total mass of the robot, and $H(t)$ is the horizontal reaction force. Also, the translational take-off velocity, (12), and the angular velocity, (13), are given as follows:

$$m_{\text{robot}} v_{\text{robot}} = \sum_{i=1}^6 m_i v_{i,f} \quad (12)$$

$$\omega_{\text{robot}} = \sum_{i=1}^6 m_i c_i \omega_{i,f} / \sum_{i=1}^6 m_i c_i \quad (13)$$

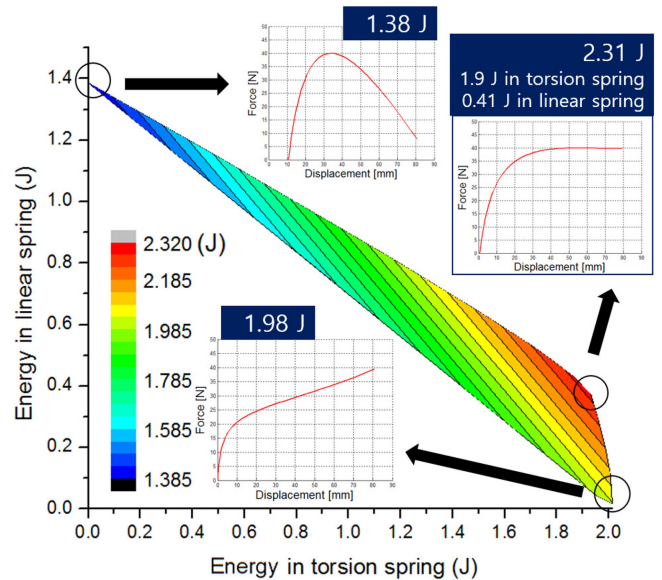


Fig. 10. Stored energy in a linear spring versus stored energy in a torsional spring under limited structural robustness of 40 N.

where ω_{robot} is the angular velocity, v_{robot} is the velocity of the mass center, $\omega_{i,f}$ is the angular velocity, c_i is the position of a mass center, and $v_{i,f}$ is the translational velocity of each link just before takeoff.

IV. RESULTS

How to combine different types of energy storages is important for the robot to maximally save the energy under the limit of structural robustness. To investigate the influence of each energy storage and find the best combination, several curves of loading force depending on the displacement are derived and optimized based on the modeling.

The determined combination of the linear springs and the torsional springs are applied to the jumping module and the module is tested to check the jumping ability. Also, to confirm the functionality of the clutch mechanism and to show the height-adjustability of the jumping module, several jumps are done by varying the amount of stored energy.

The optimized jumping module is combined into the crawling robot. To investigate trajectory adjustability, the integrated jumping–crawling robot is tested by varying the jumping speed and the crawling speed. In addition, the self-righting shell is added to the robot to show the usability in real-world applications.

A. Maximizing Storable Energy

The best combination of the linear springs and the torsional springs is examined by only varying the spring constants since the amount of deformation of the springs is fixed by the geometry.

Fig. 10 shows the amount of storable energy when the limit of the structural robustness is given as 40 N—all cases in Fig. 10 has the limit of 40 N. When the module employs a linear spring

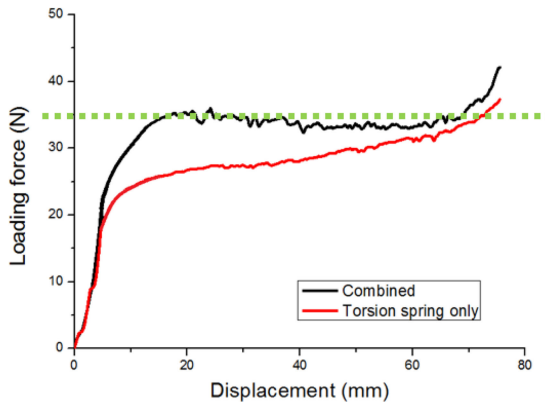


Fig. 11. Experimental results of loading force versus displacement.

only, the loading force rapidly increases to the peak and drops toward zero. In this case, the module can store 1.38 J. When the module uses a torsional spring only, the loading force steadily increases to 40 N and the module stores the energy of 1.98 J. In case of the optimized case, the jumping module can maximally utilize the area under the limit and store the energy up to 2.31 J, as shown in Fig. 10.

Based on the investigation, the spring constants of the linear spring and the torsional spring are determined as 400 N/m and 0.6 Nm/rad, respectively. In this case, the jumping module is designed to have force limit of 35 N, considering the safety factor. To check the loading force profile, the force required to load the energy is measured by varying the displacement, as shown in Fig. 11. The torsional spring only case (spring constant of 1.68 Nm/rad) shows a rapid increase of the loading force at the beginning and rises up to the limit of the structural robustness. In case of the optimized combination, the overall trend of the loading force curve shows good agreement with that of the modeling. As a result, the optimized jumping module stores the energy of 1.75 J, whereas the torsional spring only case stores 1.35 J.

The results are also confirmed through jumping experiments and dynamic modeling. Fig. 13(a) and (b) shows high-speed images and corresponding dynamic models. In Fig. 13(a), the module store 1.35 J in torsional spring, whereas the optimized module stores 1.75 J in both torsion and linear springs. In Fig. 13(a), the module jumps within 14 ms with a launching speed of 6.93 m/s and jumps to 2.4 m, as shown in Fig. 12(a). The module actually uses 1.06 J, which is 78.7% of its initially stored energy. On the other hand, the optimized jumping module in Fig. 13(b) takes off within 15 ms with a speed of 7.86 m/s and jumps to the height of 3.1 m, as shown in Fig. 12(b). The optimized module uses 1.38 J in reality, which is 79.0% of the initially stored energy.

The difference of the jumping performance can be explained based on the ground reaction in Fig. 13(a) and (b) (left column). Fundamentally, launching speed of a jumping module is determined by the transferred momentum given by the multiplication of the reaction force and the time. If we look at the reaction force

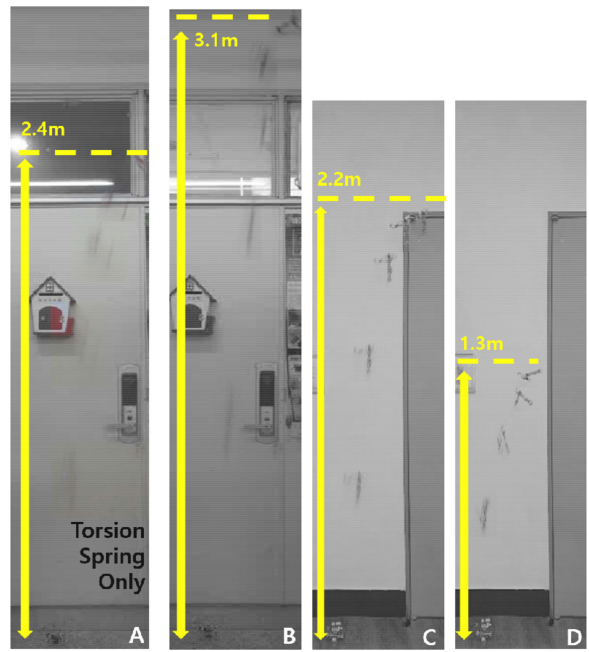


Fig. 12. Maximum jumping height depending on types of energy storages such as (a) torsional spring only and (b) optimally combined case. (b)–(d) Height-adjustable jumping. The module can adjust jumping height from 0 to 3.1 m using the active clutch mechanism. The module has initially stored energy of (b) 1.75 J, (c) 1.24 J, and (b) 0.75 J, each.

curve of both cases, the optimized case has a larger area under the curve of the vertical reaction force. Therefore, the optimized module jumps better than the module with the torsional spring only.

B. Height-Adjustable Jumping

Ability to adjust the take-off speed and the jumping height is essential for the integrated jumping–crawling robot to get the desired launching trajectory. To check the height adjustability, several jumps are implemented by varying the amount of stored energy using the clutch mechanism.

Fig. 13(b)–(d) show high-speed images and corresponding dynamic models. In Fig. 13(b), the module is fully compressed and stores the energy of 1.75 J. The jumping module takes off within 15 ms with a launching speed of 7.86 m/s and jumps to 3.1 m, as shown in Fig. 12(b). The module in Fig. 13(c) is compressed two-third of the fully compressed state and stores the energy of 1.24 J. The module launches within 10 ms with a take-off speed of 6.61 m/s and jumps to 2.2 m, as shown in Fig. 12(c). The module actually uses 0.96 J, which is 78.3% of its initially stored energy. Fig. 13(d) is compressed one-third of the fully compressed state and stores the energy of 0.74 J. The module launches within 7 ms with a take-off speed of 5.07 m/s and jumps to 1.3 m, as shown in Fig. 12(d). The module actually uses 0.58 J, which is 78.2% of its initially stored energy. In summary, the module jumps earlier when the module stores less energy and launches with low speed.

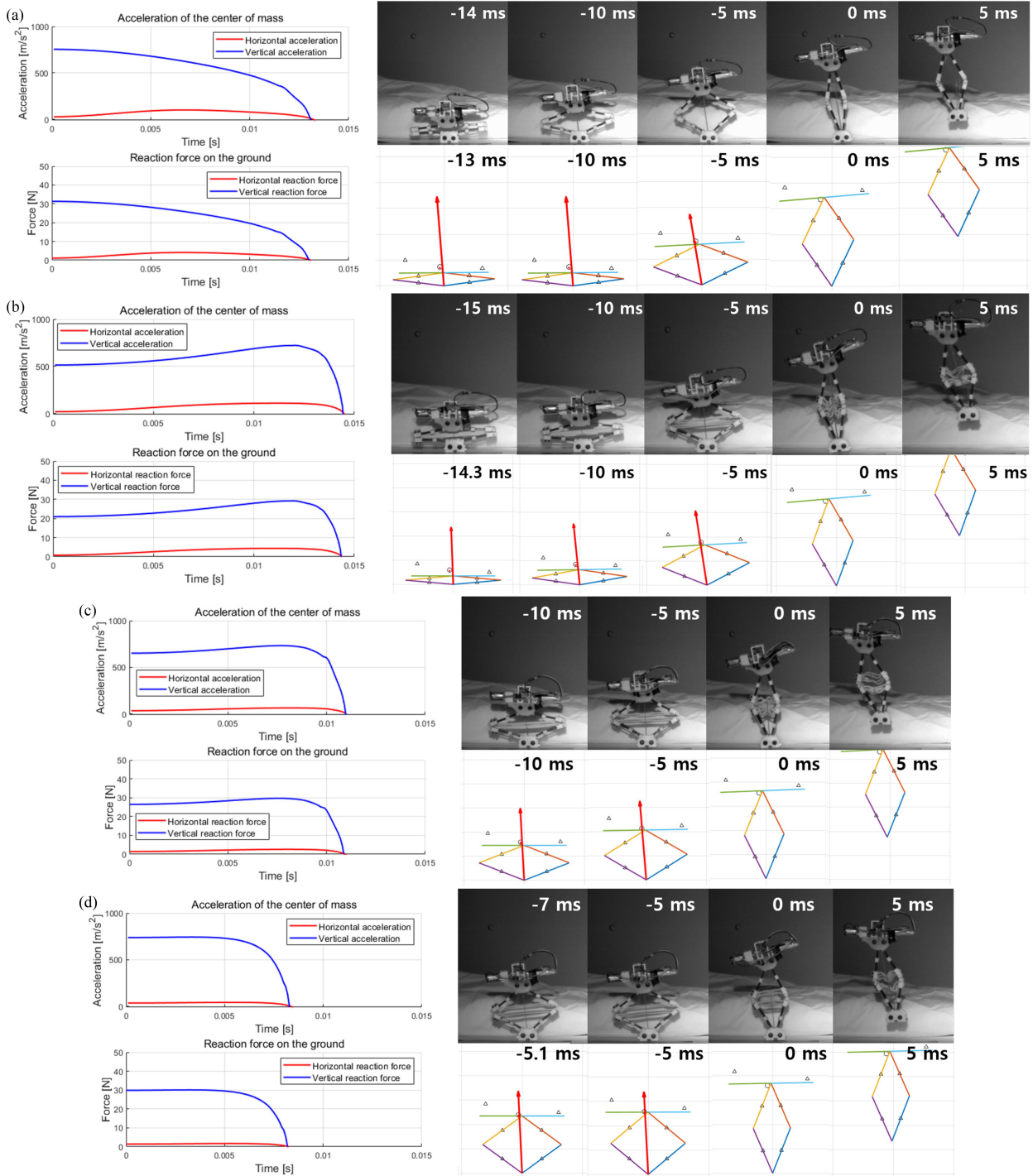


Fig. 13. Acceleration, ground reaction force, visualization of dynamic modeling, and high-speed (1000 fps) images of the jumping module. The red arrow indicates the direction of the reaction force from the ground. (a) Jumping module with torsional springs only. (b)–(d) Height-adjustable jumping with initially stored energy of (b) 1.75 J, (c) 1.24 J, and (b) 0.75 J, each.

The difference in take-off speeds can be also understood to see the left column of Fig. 13(b), (c), and (d), which shows the ground reaction force of each jump. As shown in the graphs, the fully compressed case has the maximum area under the curve and transfers the largest momentum to the jumping module. As the quantity of stored energy decreases, the area under the

curve and the transferred momentum reduces. This results in the decrease in take-off speed and jumping height.

C. Trajectory-Adjustable Jumping-Crawling

The JumpRoACH is tested to show trajectory-adjustability by changing the take-off speed and the crawling speed.

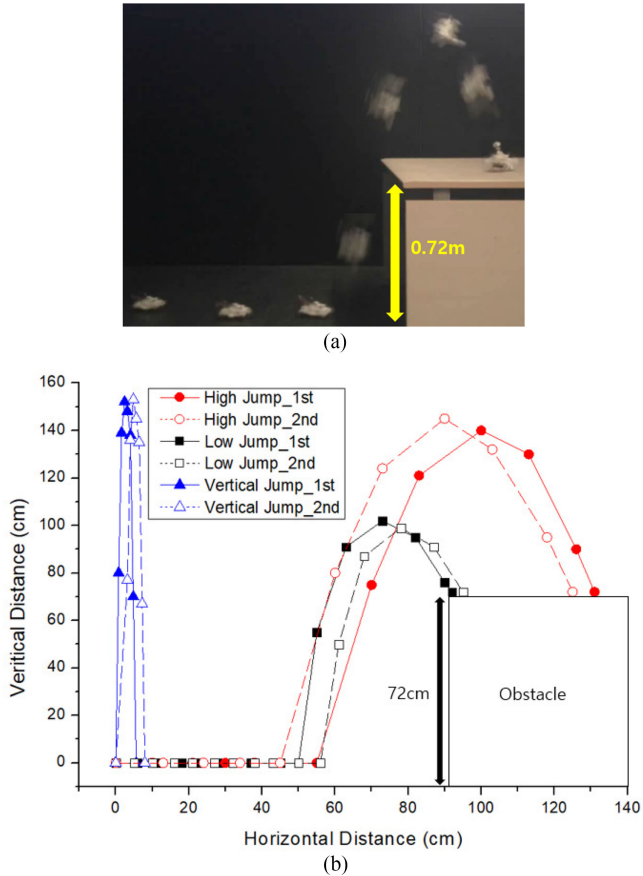


Fig. 14. (a) Integrated jumping–crawling to overcome an 0.72-m obstacle. (b) Vertical and horizontal distance of the integrated jumping–crawling robot. The time between dots is 0.168 s.

Fig. 14(a) indicates the robot that crawls 0.56 m/s and takes off 5.39 m/s. Thanks to the integrated motion, the robot jumps 1.5 m, crawls 0.76 m, and overcomes a 0.72-m high obstacle.

Fig. 14(b) indicates the distance in horizontal and vertical directions of three cases. All cases are repeated twice to check the repeatability of the jumping trajectory and the corresponding data are given in Table V. Overall, all cases show similar jumping trajectories when the robot is set to have equal initial energy and crawling speed.

In vertical jumping case, the robot is set to crawl at 0 m/s and the jumping module has the initially stored energy of 1.75 J, which is fully compressed state. The robot takes off with the speed of around 5.5 m/s and jumps about 1.5 m toward nearly vertical direction. In low jumping case, the robot has initial energy of 1.22 J and is set to crawl at about 0.3 m/s. The robot jumps to about 1.0 m with the take-off speed of around 4.5 m/s and moves about 0.4 m horizontally. In high jumping case, the robot is set to crawl at about 0.55 m/s and has initially stored energy of 1.75 J. The robot jumps to about 1.45 m with the take-off speed of around 5.4 m/s and moves about 0.75 m horizontally.

Fig. 15 shows the adjustable jumping range of the JumpRoACH. The amount of stored energy can be adjusted until

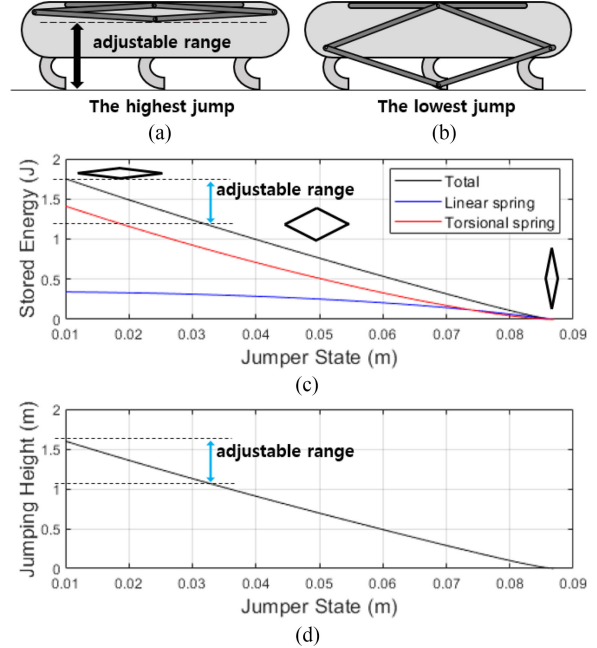


Fig 15. (a) and (b) Adjustable range of the jumper. (c) Adjustable range of storables energy. (d) Corresponding jumping range.

the jumper does not hinder the crawling locomotion. Fig. 15(a) and (b) indicates the highest and the lowest jumping cases, respectively. If the jumper unfolds more from the state shown in Fig. 15(b), then the crawler's legs begin to be in the air and cannot crawl.

Fig. 15(c) and (d) shows the calculated stored energy based on the static model and the corresponding jumping height, respectively. As shown in the graphs, the JumpRoACH can adjust the jumping height from 1.11 to 1.60 m, which corresponds to the stored energy from 1.22 to 1.75 J. In case of crawling speed, the JumpRoACH can adjust the speed from 0 to 0.56 m/s regardless of the jumping height. Consequently, moving trajectories can be made by combining the jumping speed from 4.64 to 5.60 m/s and the crawling speed from 0 to 0.56 m/s.

To prove usability in real-world applications, the robot is tested on the cluttered terrain, as shown in Fig. 16. The target place is located at the height of 1.6 m. To reach the target, the robot needs to jump twice. Therefore, the robot implements the first jump, stands upright itself, and jumps again toward the target. By doing so, the robot finally reaches the target place, as shown in Fig. 16(e).

The operating time is dependent on scenarios since each mode requires different amount of energy consumption. Crawling with the maximum speed needs continuous current of 1.26 A (0.63 A for each crawling motor). The loading of the jumper requires continuous current of 0.84 A during 50 s, which is full loading time. Considering that the battery used for the JumpRoACH is 150 mAh, the JumpRoACH crawls about 5 min when the robot only runs. When the robot only jumps, about nine jumps are done. If the robot needs to jump twice, as shown in Fig. 16, the JumpRoACH crawls for about 4 min.

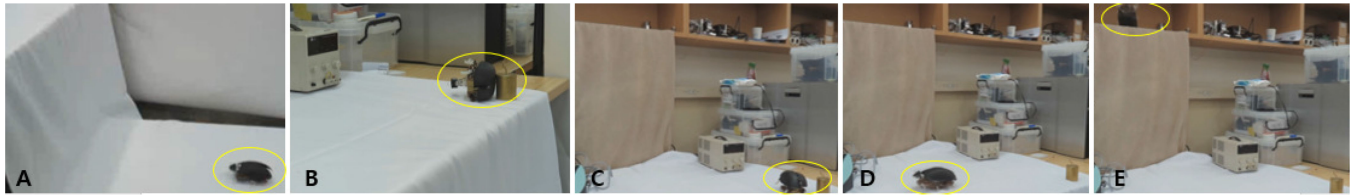


Fig. 16. Reaching target place through integrated jumping–crawling and self-righting. The robot (a) overcomes an 0.90-m obstacle, (b) and (c) stands upright itself, and (d) maneuvers toward the target. (e) Robot jumps again and finally, reaches the target.

TABLE IV
COMPARISON OF EXPERIMENT AND MODELING

	Jump with torsion spring only		3.1m Jump		2.2m Jump		1.3m Jump	
	Model	Experiment	Model	Experiment	Model	Experiment	Model	Experiment
Take-off time (ms)	13.0	14.0	14.3	15.0	10.8	10.0	8.1	8.0
Vertical take-off speed(m/s)	7.53	6.93	8.50	7.86	7.18	6.61	5.52	5.07
Initially stored energy (J)	1.35	1.35	1.75	1.75	1.24	1.24	0.74	0.74
Actual used energy (J)	1.18	1.06	1.48	1.38	1.03	0.96	0.60	0.58
Conversion efficiency (%)*	87.5	78.7	84.7	79.0	83.4	78.3	81.9	78.2
Jumping height (m)	-	2.4	-	3.1	-	2.2	-	1.3

*Conversion efficiency is the ratio of initially stored energy to actual kinetic energy at take-off [1], [12].

TABLE V
EXPERIMENTAL DATA OF INTEGRATED JUMPING–CRAWLING

	High Jump		Low Jump		Vertical Jump	
	1 st try	2 nd try	1 st try	2 nd try	1 st try	2 nd try
Initially stored energy (J)	1.75	1.75	1.22	1.22	1.75	1.75
Actual take-off speed (m/s)	5.39	5.41	4.52	4.50	5.56	5.57
Actual Jumping height (m)	1.40	1.44	1.02	0.99	1.52	1.53
Initially set crawling speed (m/s)	0.56	0.55	0.32	0.30	0.00	0.00
Horizontal travel distance (m)	0.76	0.80	0.43	0.39	0.06	0.08

V. DISCUSSION

We discuss two issues in this section. First, the difference between data from the experimental and the model is examined. Second, the relation between the energy storing method and the curve trend of the acceleration and the ground reaction force is investigated.

Table IV compares the experimental and the modeling data. Both sets of data show good agreement in overall trend but slight differences in detail numbers. If we look at the conversion efficiency, which means the ratio of the initially stored energy to the actually used energy, the module uses less energy in actual jumping. Because of less energy conversion, the real jumping shows 2% to 3% of decreased performance in the take-off speed and the jumping height. Probably, this error is originated from a small degree of hysteresis in the energy storing elements such as the latex rubber and the torsional springs. These elements are modeled as ideal springs in the modeling and this results in better performance compared with that of real experiments.

The left column of **Fig. 13** shows curves of the acceleration and the ground reaction force from dynamic modeling. The graphs in **Fig. 13**, however, indicate different appearances depending on the types of energy storages and the ratio of energy storages. To begin with, the module with only torsion springs in **Fig. 13(a)** shows the maximum value at the beginning and the value gradually decreases to zero. On the other hand, the optimized module in **Fig. 13(b)** shows a steady increase to the peak and rapidly drops to zero. This is because of difference in types of energy storages. In case of the torsional springs, the maximum normal force is exerted on the ground when the module is fully compressed. In case of the linear springs, however, 0 N of normal force is exerted on the ground when the module is in the fully compressed position since the moment arm is zero. As the jumping module starts to unfold, the moment arm increases and accordingly the reaction force rises to peak, as shown in **Fig. 13(b)**.

Fig. 13(b)–(d) shows the curves of height-adjustable jumping and each case has the initially stored energy of 1.75, 1.24, and 0.74 J, respectively. As the quantity of the initially stored energy decreases, the shape of the curve becomes similar to that of the module with torsion springs only. When the optimized jumping module stores less energy, the module is less compressed. That is, the moment arm of the torque induced by the linear spring is not zero and accordingly, the module initially has a certain amount of ground reaction force. Therefore, the initial value of the ground reaction force gets larger as the module stores less energy.

VI. CONCLUSION

In this paper, we proposed a trajectory-adjustable integrated jumping–crawling robot called JumpRoACH. The key issue was how to maximize the energy-storing capacity of the jumping module in the confined space since the jumping module was

required to be installed in a tiny space located inside the crawler's body. To resolve this issues, the jumping module was designed to incorporate different types of energy-storing components such as linear springs and torsional springs. By appropriately combining those two types of springs, the jumping module could maximally use the area under the limit of structural robustness. Therefore, the jumping module could achieve the energy density of 30.9 J/g and enabled the JumpRoACH to jump up to the height of 1.52 m.

Also, an active clutch mechanism was designed to store the release the energy in any state. The clutch works based on a single dc motor and operates by changing the direction of rotation. Thanks to the clutch, the jumping module could adjust both jumping height and timing. In addition, an active shell was designed to upright the robot itself. Finally, the jumping module, the active shell, and the lightweight VelociRoACH crawler were integrated together as a single multimodal robot. Through the several experiments, we have shown that the whole system achieves different trajectories and have potential to be used in real-world applications.

REFERENCES

- [1] J. Burdick and P. Fiorini, "Minimalist jumping robots for celestial exploration," *Int. J. Robot. Res.*, vol. 22, no. 7/8, pp. 653–674, 2003.
- [2] M. A. Woodward and M. Sitti, "MultiMo-Bat: A biologically inspired integrated jumping-gliding robot," *Int. J. Robot. Res.*, vol. 33, no. 12, pp. 1511–1529, 2014.
- [3] A. Vidyasagar, J. C. Zufferey, D. Floreano, and M. Kovac, "Performance analysis of jump-gliding locomotion for miniature robotics," *Bioinspiration Biomimetics*, vol. 10, no. 2, 2015, Art. no. 025006.
- [4] A. L. Desbiens, M. T. Pope, D. L. Christensen, E. W. Hawkes, and M. R. Cutkosky, "Design principles for efficient, repeated jumpgliding," *Bioinspiration Biomimetics*, vol. 9, no. 2, Jun. 2014, Art. no. 025009.
- [5] M. Kovac, "EPFL jumpglider: A hybrid jumping and gliding robot with rigid or folding wings," in *Proc. IEEE/RSJ Int. Conf. Robot. Biomimetics*, 2011, pp. 1503–1508.
- [6] M. A. Woodward and M. Sitti, "Design of a miniature integrated multimodal jumping and gliding robot," (in English), in *Proc. IEEE/RSJ Int. Conf. Intell. Robots Syst.*, 2011, pp. 556–561.
- [7] S. A. Stoeter and N. Papanikopoulos, "Kinematic motion model for jumping scout robots," *IEEE Trans. Robot.*, vol. 22, no. 2, pp. 397–402, Apr. 2006.
- [8] J. Zhao *et al.*, "MSU Jumper: A single-motor-actuated miniature steerable jumping robot," *IEEE Trans. Robot.*, vol. 29, no. 3, pp. 602–614, Jun. 2013.
- [9] R. Armour, K. Paskins, A. Bowyer, J. Vincent, and W. Megill, "Jumping robots: A biomimetic solution to locomotion across rough terrain," *Bioinspiration Biomimetics*, vol. 2, pp. S65–S82, 2007.
- [10] H. Tsukagoshi, M. Sasaki, A. Kitagawa, and T. Tanaka, "Design of a higher jumping rescue robot with the optimized pneumatic drive," in *Proc. IEEE Int. Conf. Robot. Autom.*, 2005, pp. 1276–1283.
- [11] B. G. A. Lambrecht, A. D. Horchler, and R. D. Quinn, "A small, insect-inspired robot that runs and jumps," in *Proc. IEEE Int. Conf. Robot. Autom.*, 2005, pp. 1240–1245.
- [12] G. P. Jung, J. S. Kim, J. S. Koh, S. P. Jung, and K. J. Cho, "Role of compliant leg in the flea-inspired jumping mechanism," in *Proc. IEEE/RSJ Int. Conf. Intell. Robots Syst.*, 2014, pp. 315–320.
- [13] Y. Sugiyama and S. Hirai, "Crawling and jumping by a deformable robot," *Int. J. Robot. Res.*, vol. 25, no. 5/6, pp. 603–620, 2006.
- [14] A. Yamada, M. Watari, H. Mochiyama, and H. Fujimoto, "An asymmetric robotic catapult based on the closed elastica for jumping robot," in *Proc. IEEE Int. Conf. Robot. Autom.*, 2008, pp. 232–237.
- [15] M. Noh, S. W. Kim, S. An, J. S. Koh, and K. J. Cho, "Flea-inspired catapult mechanism for miniature jumping robots," *IEEE Trans. Robot.*, vol. 28, no. 5, pp. 1007–1018, Oct. 2012.
- [16] S.-M. An, J. Ryu, M. Cho, and K.-J. Cho, "Engineering design framework for a shape memory alloy coil spring actuator using a static two-state model," *Smart Mater. Struct.*, vol. 21, no. 5, 2012, Art. no. 055009.
- [17] K. Otsuka and C. M. Wayman, *Shape Memory Materials*. Cambridge, U.K.: Cambridge Univ. Press, 1999.
- [18] J. Zhao, W. Yan, N. Xi, M. W. Mutka, and L. Xiao, "A miniature 25 grams running and jumping robot," in *Proc. IEEE Int. Conf. Robot. Autom.*, 2014, pp. 5115–5120.
- [19] M. Kovac, M. Fuchs, A. Guignard, J. C. Zufferey, and D. Floreano, "A miniature 7 g jumping robot," in *Proc. IEEE Int. Conf. Robot. Autom.*, 2008, pp. 373–378.
- [20] M. Kashki, J. Zoghzoghy, and Y. Hurmuzlu, "Adaptive control of inertially actuated bouncing robot," *IEEE/ASME Trans. Mechatronics*, vol. 22, no. 5, pp. 2196–2207, Oct. 2017.
- [21] D. W. Haldane, M. M. Plecnik, J. K. Yim, and R. S. Fearing, "Robotic vertical jumping agility via series-elastic power modulation," *Sci. Robot.*, vol. 1, no. 1, 2016, Art. no. eaag2048.
- [22] Z. Batts, J. Kim, and K. Yamane, "Design of a hopping mechanism using a voice coil actuator: Linear elastic actuator in parallel (LEAP)," in *Proc. IEEE Int. Conf. Robot. Autom.*, 2016, pp. 655–660.
- [23] U. Scarfogliero, C. Stefanini, and P. Dario, "Design and development of the long-jumping "Grillo" mini robot," in *Proc. IEEE Int. Conf. Robot. Autom.*, 2007, pp. 467–472.
- [24] F. Li *et al.*, "Jumping like an insect: Design and dynamic optimization of a jumping mini robot based on bio-mimetic inspiration," *Mechatronics*, vol. 22, no. 2, pp. 167–176, 2012.
- [25] V. Zaitsev, O. Gvirzman, U. Ben Hanan, A. Weiss, A. Ayali, and G. Kosa, "A locust-inspired miniature jumping robot," *Bioinspiration Biomimetics*, vol. 10, no. 6, Nov. 2015, Art. no. 066012.
- [26] A. Beck, V. Zaitsev, U. B. Hanan, G. Kosa, A. Ayali, and A. Weiss, "Jump stabilization and landing control by wing-spreading of a locust-inspired jumper," *Bioinspiration Biomimetics*, vol. 12, no. 6, 2017, Art. no. 066006.
- [27] M. T. Tolley *et al.*, "An untethered jumping soft robot," in *Proc. IEEE/RSJ Int. Conf. Intell. Robots Syst.*, 2014, pp. 561–566.
- [28] G.-P. Jung, C. S. Casarez, S.-P. Jung, R. S. Fearing, and K.-J. Cho, "An integrated jumping-crawling robot using height-adjustable jumping module," in *Proc. IEEE Int. Conf. Robot. Autom.*, 2016, pp. 4680–4685.
- [29] D. W. Haldane, K. C. Peterson, F. L. G. Bermudez, and R. S. Fearing, "Animal-inspired design and aerodynamic stabilization of a hexapedal millirobot," in *Proc. IEEE Int. Conf. Robot. Autom.*, 2013, pp. 3279–3286.
- [30] E. Pena, B. Calvo, M. Martinez, and M. Doblar, "A three-dimensional finite element analysis of the combined behavior of ligaments and menisci in the healthy human knee joint," *J. Biomech.*, vol. 39, no. 9, pp. 1686–1701, 2006.
- [31] S. S. Baek, F. L. G. Bermudez, and R. S. Fearing, "Flight control for target seeking by 13 gram ornithopter," in *Proc. IEEE/RSJ Int. Conf. Intell. Robots Syst.*, 2011, pp. 2674–2681.
- [32] C. Li, C. C. Kessens, R. S. Fearing, and R. J. Full, "Mechanical principles of dynamic terrestrial self-righting using wings," *Adv. Robot.*, vol. 31, no. 17, pp. 881–900, 2017.



Gwang-Pil Jung received the B.S. degree from the KAIST, Daejeon, South Korea, in 2010, and the Ph.D. degree from Seoul National University, Seoul, South Korea, in 2016, both in mechanical engineering.

He is currently an Assistant Professor in mechanical and automotive engineering and the Director of Bio-Inspired Design Laboratory, SeoulTech, Seoul, South Korea. His current research interests include design and fabrication of milliscale biologically inspired robots.



Carlos S. Casarez received the B.S. degree in mechanical engineering from the University of Maryland, College Park, College Park, MD, USA, in 2013, and the M.S. and Ph.D. degrees in mechanical engineering from the University of California, Berkeley, Berkeley, CA, USA, in 2016 and 2018, respectively.

He is currently a robotic controls Engineer with Intuitive Surgical, Sunnyvale, CA, USA.



Soo-Hwan Chae received the B.S. degree in mechanical engineering in 2017 from Seoul National University, Seoul, South Korea, where he is currently working toward the Ph.D. degree in mechanical engineering at the Biorobotics Laboratory.

His current research interests include the design and fabrication of biologically inspired robots.



Jongeun Lee received the B.S. degree in mechanical engineering in 2016 from Seoul National University, Seoul, South Korea, where he is currently working toward the Ph.D. degree in mechanical engineering at the Biorobotics Laboratory.

His current research interests include the design and fabrication of biologically inspired robots.



Ronald S. Fearing received the S.B. and S.M. degrees in electrical engineering and computer science from the Massachusetts Institute of Technology, Cambridge, MA, USA, in 1983, and the Ph.D. degree in electrical engineering from Stanford University, Stanford, CA, USA, in 1988.

He is currently a Professor with the Department of Electrical Engineering and Computer Sciences, University of California, Berkeley, Berkeley, CA, USA, which he joined in January 1988. His research interests include

millirobotics, including flying and crawling millirobots, multirobot dexterous manipulation, parallel nanograsping (gecko adhesion), and rapid prototyping. He has also worked in tactile sensing, teletaction, and multifinger dexterous manipulation. He holds 17 U.S. and international patents.

Dr. Fearing was a recipient of the Presidential Young Investigator Award in 1991.



Sang-Min Baek received the B.S. degree in mechanical engineering from the KAIST, Daejeon, South Korea, in 2014. He is currently working toward the Ph.D. degree in mechanical engineering at the Biorobotics Laboratory, Seoul National University, Seoul, South Korea.

His current research interests include the design and fabrication of biologically inspired robots.



Kyu-Jin Cho received the B.S. and M.S. degrees from Seoul National University, Seoul, South Korea, in 1998 and 2000, respectively, and the Ph.D. degree from the Massachusetts Institute of Technology, Cambridge, MA, USA, in 2007, all in mechanical engineering.

He was a Postdoctoral Fellow with the Harvard Microrobotics Laboratory until 2008. He is currently a Professor in mechanical and aerospace engineering and the Director of Biorobotics Laboratory, and the Director of Soft

Robotics Research Center (SRRC), Seoul National University. His research interests include biologically inspired robotics, soft robotics, soft wearable robots, and rehabilitation/assistive robotics.

Prof. Cho was a recipient of the 2014 IEEE RAS Early Academic Career Award, the 2014 ASME Compliant Mechanism Award, and the 2013 IROS Best Video Award.



So-Jung Yim received B.S. degree in physics education and M.S. degree in mechanical engineering, in 2017 and 2019, respectively, from Seoul National University, Seoul, South Korea, where she is currently working toward the Ph.D. degree in mechanical engineering at the Biorobotics Laboratory.

Her current research interests include the design and fabrication of biologically inspired robots.